Final Project ST5

Slim Barkallah

November 2023

1 Control of acoustic wave by changing the geometry on a surface

In this part, I will present the resolution of a Helmholtz equation for various geometries and analyze the error for different values of the wave number.

Consider a domain $\Omega = [0,1] \times [0,1]$ with $\partial\Omega = \Gamma_d \cup \Gamma_n$, where Γ_d represents the left boundary. The Helmholtz equation with Dirichlet boundary conditions is given by:

$$\Delta u + k^2 u = f, \quad in\Omega$$

$$u = 0, \quad on\Gamma_d$$

$$\frac{\partial u}{\partial n} = 0, \quad on\Gamma_n$$

In this context, we will consider $f(x,y) = \left(\pi^2 \times \frac{5}{4} - k^2\right) \times \sin\left(\frac{\pi}{2} \times x\right) \times \cos(\pi \times y)$.

1.1 Analytical resolution

Using the separation of variables method, we can prove that the analytical solutions of the Helmholtz equation with this mixture of Neumann and Dirichlet conditions are the functions

$$\phi(x,y) = A \cdot \sin\left(\left(n + \frac{1}{2}\right)\pi x\right) \cdot \cos(m\pi y) + \sin\left(\frac{\pi}{2}x\right) \cdot \cos(\pi y).$$

Here, A is a constant, and n and m are integers verifying the condition $\left(\left(n + \frac{1}{2}\right) + m^2\right) \cdot \pi^2 = k^2$.

It's worth noting that the solution is not unique due to the lack of uniqueness of the solution. However, if we fix k as a multiple of π or if k is complex, the condition $\left(\left(n + \frac{1}{2}\right) + m^2\right) \cdot \pi^2 = k^2$ cannot hold. This imposes that $A = 0$, and our solution will be unique:

$$\phi(x,y) = \sin\left(\frac{\pi}{2}x\right) \cdot \cos(\pi y).$$

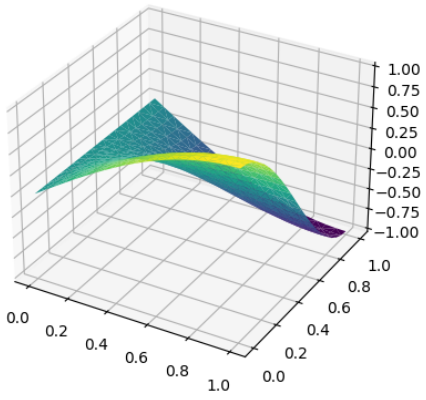

Figure 1: Exact solution of the problem $\phi(x, y) = \sin\left(\frac{\pi}{2}x\right) \cdot \cos(\pi y)$

1.2 Numerical resolution

In the numerical resolution of this method, I will consider two approaches. The first one involves a square triangle mesh, and the second one involves an irregular geometry. Our goal is to study the effects of the change in geometry on the approximate solution and the eigenvalues of the equation.

1.2.1 Regular geometry

We consider a squared $n \times n$ triangle mesh. The idea is to use the finite difference method to solve the equation. There are two types of conditions on the boundary: Neumann and Dirichlet.

Let's denote the matrices X, A, and B, and those of the linear system that we will solve. X is an $(n+1)$-dimensional vector. We denote X_i as the value of X at node i. x_i, y_i, and z_i are the coordinates of node i.

I will discuss how these boundary conditions are imposed on the final solution.

1.2.2 Dirichlet Condition

For Dirichlet conditions, we choose to fix the value $X_i = 0$ for all the nodes on the west boundary. This condition can be imposed by ensuring that the ith row of matrix A contains one non-zero element at the ith index, and we fix $b_i = 0$. Alternatively, we can use the method elaborated in the function `_set_dirichlet_condition`.

It is worth noting that using the Dirichlet condition on the west boundary without imposing Neumann conditions gives the desired result, which may suggest that Neumann conditions are unnecessary as they add small uncertainty

to the problem. However, this conjecture was only observed on regular meshes. We will explore this further in paragraph 1.2.7.

Neumann conditions We need to impose that the derivative of the function is equal to zero on the boundary. Let p_i denote the node that is just near node i in the direction of the gradient vector, where i is a node on the Neumann boundary Γ_n. For example, $p_i = i$ for nodes in the east boundary, and for the other parts of the boundary, $p_i = \pm(n-1) + i$.

We can then use the Taylor series and the fact that $|x_i - x_{p_i}| = \frac{1}{n}$ to approximate:

$$\phi(x_{i-1}, y) = \phi(x_i, y) - \frac{1}{n}\frac{\partial \phi}{\partial x}(x_i, y),$$

for all $y \in [0, 1]$. We want $\phi(x_i) = X_i$, so we impose $X_i = X_{p_i}$ by changing the coefficients of A and B.

Hence, we can solve the resulting linear system, and we obtain a numerical solution as shown in Figure 2. We then studied the influence of the wave number on the error. When the modulus of k goes to ∞, the error approaches zero, as presented in Figure 3.

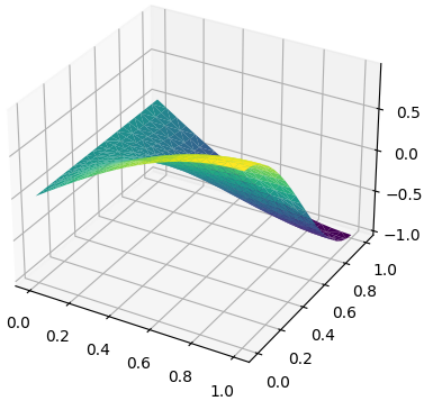

Figure 2: Numerical solution

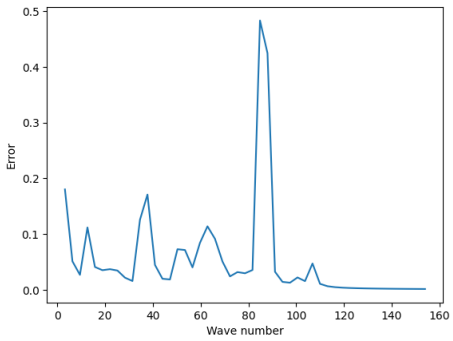

Figure 3: Norm L^2 of the error as a function of the modulus of the wave number

1.2.3 Identifying Localized Eigenmodes

In this part, I will study the approximated eigenvalues of the Helmholtz equation. I choose to fix the wave number $k = 10\pi$, and we will fix $n = 20$ (a 20×20 mesh).

I have noticed that all the eigenvalues are real. So, plotting the real part as a function of the imaginary part does not provide valuable information. Instead, Figure 4 represents the eigenvalues, and we can observe that a priori there exist two classes of eigenvalues. At this stage, I hypothesize that these two classes correspond to localized and non-localized modes.

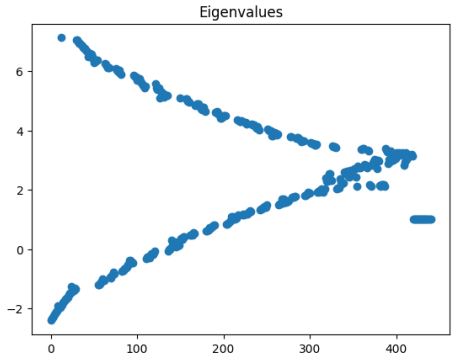

Figure 4: Eigenvalues of the Helmholtz equation on a squared 20×20 triangle mesh

1.2.4 Visualization

To test this conjecture, I began by visualizing 300 out of 441 eigenvectors and manually noted the modes that are localized and those that are not localized. Figures 5 and 6 show examples of the represented eigenvalues.

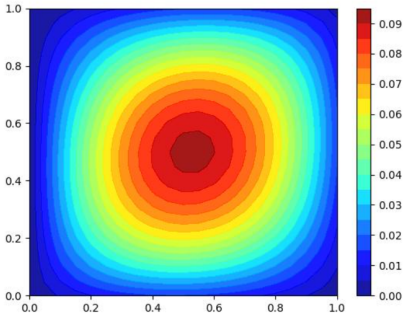

Figure 5: Localized eigenmode

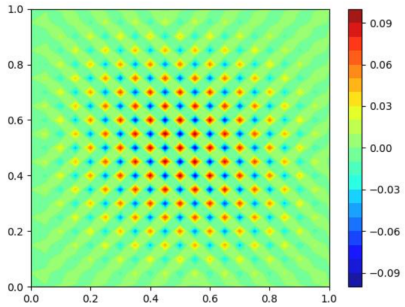

Figure 6: Non-localized eigenmode

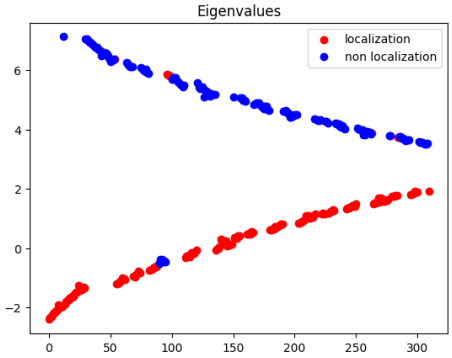

Figure 7: Labeled eigenvalues of the Helmholtz equation.

I stopped at 300 eigenmodes because beyond that point, it became difficult to distinguish whether a mode is localized or not.

1.2.5 Energy Loss

Here we have two approaches that will give the same result. Either we consider that eigenvectors are normalized, and we take $S = (n+1)^2$, or $S = 1$ and normalize the eigenvectors, assuming that S represents the physical surface of a square with width 1. I adopt the second approach and multiply the eigenvector by $(n+1)$ to ensure that $\int_\Gamma 1 ds = \frac{1}{(n+1)^2} \sum_{i=1}^{i=(n+1)^2} 1 = S$.

Figure 8 represents the energy loss for different eigenmodes, and we can observe that the more localized the mode is, the greater the losses it provides. It is worth noting that there are some exceptions, which could be caused by incorrect labeling during visualization.

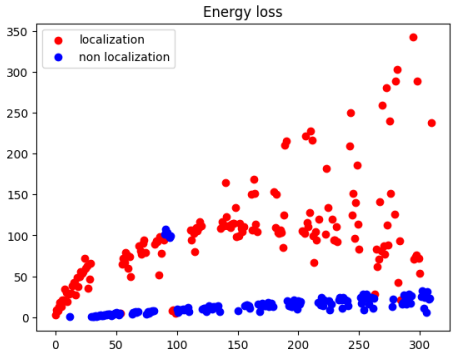

Figure 8: Energy loss

1.2.6 Irregular Geometry

In this section, I will study the eigenvalues and localization of the eigenmodes for an irregular mesh. I will use the fractal represented in Figure 9.

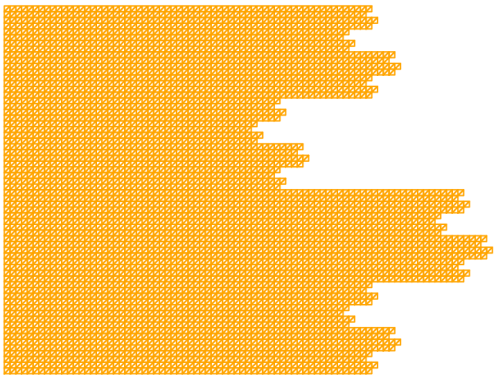

Figure 9: Irregular mesh as a fractal

1.2.7 Boundary Conditions

As I asserted in the previous section, Neumann conditions are essential to guarantee the convergence and consistency of the numerical solution. However, in this new geometry defined by the Helmholtz equation, we cannot maintain the same boundary conditions and the same function f together. This is because the analytical solutions no longer satisfy the Neumann conditions due to the change in the boundary shape and the entire resolution space. Ω is no longer $[0,1] \times [0,1]$ but is represented by the fractal.

I decided to keep the choice of the function f to enable comparison with the results of the previous section. However, I modified the Neumann condition on the boundary from zero to the derivative of the exact solution on this boundary.

Figures 10 and 11 represent the numerical solution with and without using Neumann conditions, which substantiate the aforementioned points and validate the effectiveness of the implemented approach. We must note that a new

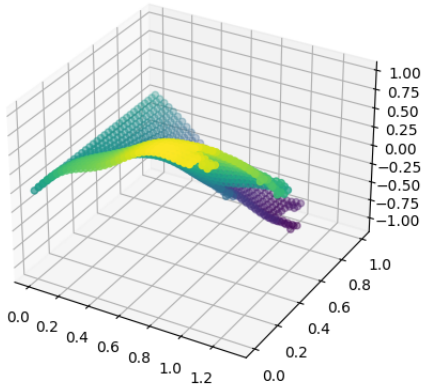

Figure 10: Numerical solution for irregular mesh with computing neuman conditions

function needs to be defined to determine the existing boundary of the irregular geometry. The principle of this function involves using the CSR representation to access the nodes corresponding to less than 6 elements, allowing us to determine the entire boundary. Subsequently, I added conditions to determine each part of the boundary.

I also created the fractal on a rectangular mesh because it was easier to compute. Then, I needed to implement a function that transforms a rectangular mesh into a triangular mesh to utilize the functions provided in the file ‘solutions.py‘.

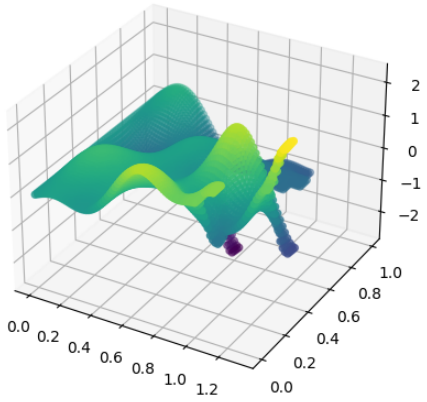

Figure 11: Numerical solution for irregular mesh without computing neuman conditions

1.2.8 Localized Modes

I have observed that all eigenvalues are real. Figure 12 presents the eigenvalues of the Helmholtz equation for an irregular mesh with $n = 64$ and the second level of fractal. Similar to the regular mesh, we observe two classes of eigenvalues indicating which modes can be localized. We utilize the energy loss to classify the eigenmodes into two distinct classes, with a threshold of 100 chosen after visualization. I also visualized the existing surfaces. Unlike a regular mesh, I was able to validate this classification using the fact that smaller exiting surfaces correspond to localized eigenmodes.

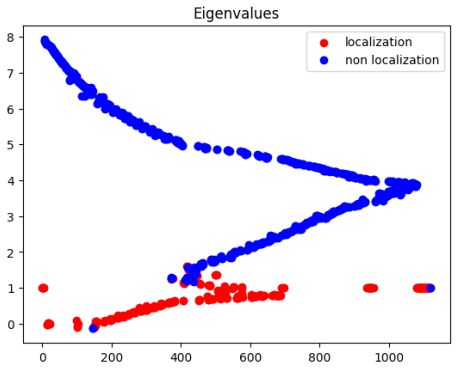

Figure 12: Eigenvalues of the Helmholtz Equation on an Irregular Mes

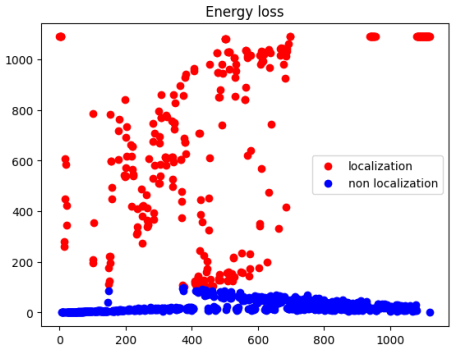

Figure 13: Energy loss

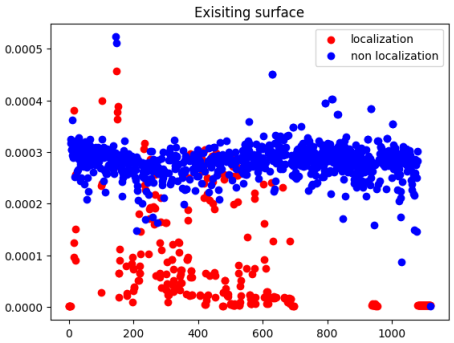

Figure 14: Existing surface

I observed that the smaller the eigenvalue, the more localized the corresponding eigenmode is. To illustrate this result, I represented the eigenvector corresponding to the smallest eigenvalue.

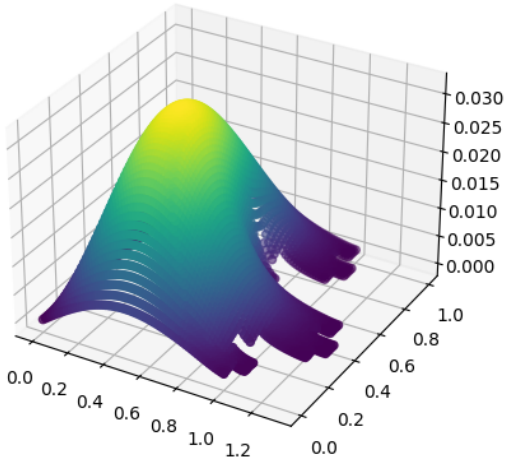

Figure 15: Eigenvector of a Localized Mode of the Helmholtz Equation on an Irregular Mesh

1.2.9 Conclusion

We can observe that the change in geometry has an impact on the resolution of the Helmholtz equation and the localized modes, including the way these modes are localized.

2 Pollution and dispersion error of the finite element method

In this part, I will present numerical solutions for the Helmholtz equation with Dirichlet conditions on the boundary. I have set fixed values at the boundary to ensure that the function $\phi(x, y) = e^{ix}$ serves as the solution to my problem. The objective of this section is to analyze the norm of the error between the numerical and analytical solutions.

2.1 Regular mesh

Let's consider a triangular mesh in the shape of a square for this part. We fix the wavenumber as $k = \pi$. Figure 16 represents the evolution of the error with h for different values of the characteristic length of the elements in the mesh. It is observed that in the logarithmic scale, a linear behavior is evident with a slope close to 1, approximately 0.99.

This confirms the theoretical result, asserting that $err = ||u^* - u_h|| \leq Ch^\alpha$ with $\alpha = 1$.

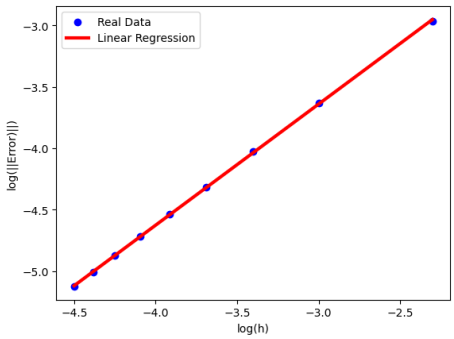

Figure 16: The error as a function of h in a log scale

Figure 17 represents the evolution of the error with k for different values of the wave number k. It is observed that in the logarithmic scale, there is a linear behavior with a slope close to 2, approximately 2.6.

This confirms the theoretical result, asserting that $err = ||u^* - u_h|| \leq Ck^\beta$ with $\beta = 2$.

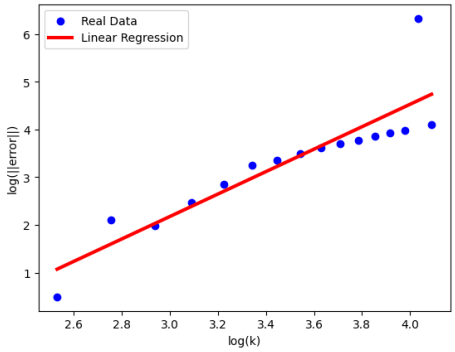

Figure 17: The error as a function of k in a log scale

2.2 Irregular mesh

In this part, I shifted the elements of the mesh using random variables. To ensure consistency in the mesh across multiple runs of the code, I generated the random variables once, setting their length compatible with the maximum number of nodes. This approach allowed for the creation of an irregular mesh while maintaining the same geometry across different program executions.

The characteristic length of the elements in the mesh was approximated by the average value of h. The results are depicted in Figures 18 and 19, where we obtained results similar to those in regular geometry, with $\alpha = 0.93$ and $\beta = 2.15$. The reduction in the α coefficient can be attributed to the

uncertainties introduced by the approximation of the characteristic length using the average.

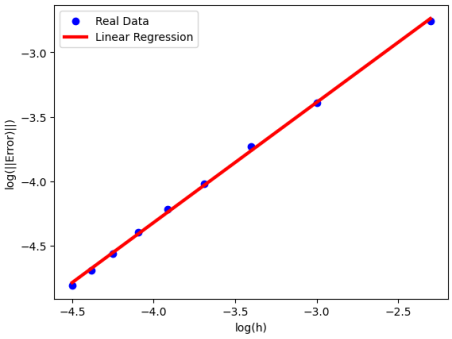

Figure 18: The error as a function of k in a log scale

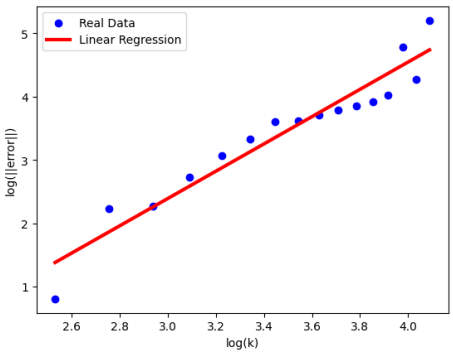

Figure 19: The error as a function of h in a log scale